Inorganic Chemistry

Article

pubs.acs.org/IC

Cooperative Effect of Unsheltered Amide Groups on CO_2 Adsorption Inside Open-Ended Channels of a Zinc(II)−Organic Framework

Cheng-Hua Lee,[†,‡] Hung-Yu Huang,[†,§] Yen-Hsiang Liu,[∥] Tzuoo-Tsair Luo,[†] Gene-Hsiang Lee,[⊥] Shie-Ming Peng,[†,⊥] Jyh-Chiang Jiang,[#] Ito Chao,*[,†] and Kuang-Lieh Lu*[,†]

[†]Institute of Chemistry, Academia Sinica, Taipei 115, Taiwan

[‡]Graduate Institute of Applied Science and Technology, National Taiwan University of Science and Technology, Taipei 106, Taiwan

[§]Department of Chemistry, National Taiwan Normal University, Taipei 116, Taiwan

[∥]Department of Chemistry, Fu Jen Catholic University, Taipei 242, Taiwan

[⊥]Department of Chemistry, National Taiwan University, Taipei 106, Taiwan

[#]Department of Chemical Engineering, National Taiwan University of Science and Technology, Taipei 106, Taiwan

Supporting Information

ABSTRACT: A unique spatial arrangement of amide groups for CO_2 adsorption is found in the open-ended channels of a zinc(II)−organic framework $\{[Zn_4(BDC)_4(BPDA)_4]\cdot 5DMF\cdot 3H_2O\}_n$ (**1**, BDC = 1,4-benzyl dicarboxylate, BPDA = *N*,*N*′-bis(4-pyridinyl)-1,4-benzenedicarboxamide). Compound **1** consists of 4^4-**sql** $[Zn_4(BDC)_4]$ sheets that are further pillared by a long linker of BPDA and forms a 3D porous framework with an α-Po $4^{12}\cdot 6^3$ topology. Remarkably, the unsheltered amide groups in **1** provide a positive cooperative effect on the adsorption of CO_2 molecules, as shown by the significant increase in the CO_2 adsorption enthalpy with increasing CO_2 uptake. At ambient condition, a 1:1 ratio of active amide sites to CO_2 molecules was observed. In addition, compound **1** favors capture of CO_2 over N_2. DFT calculations provided rationale for the intriguing 1:1 ratio of amide sorption sites to CO_2 molecules and revealed that the nanochamber of compound **1** permits the slipped-parallel arrangement of CO_2 molecules, an arrangement found in crystal and gas-phase CO_2 dimer.

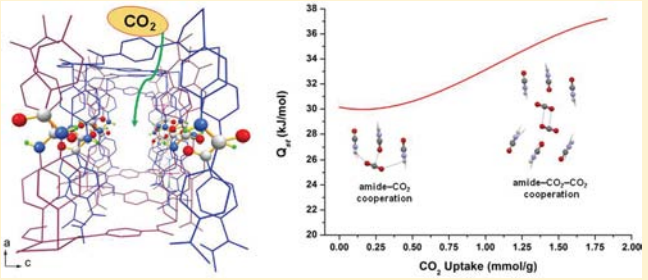

INTRODUCTION

Vigorous development of new materials for capture and storage of CO_2 is due to the fact that rapid accumulation of large amounts of CO_2 in our atmosphere has been recognized as the driving force behind the drastic climate change and global warming that we are experiencing.[1,2] Conventional methods for capture of CO_2 using amine solutions as scrubbing agents involve a high energy penalty and are inefficient in terms of releasing adsorbed CO_2 molecules.[3] Porous materials have been proposed as potential candidates for capturing CO_2. Further modification of the internal cavities of these materials with amine groups to enhance CO_2 adsorption has been investigated.[4,5] In particular, amine-mediated porous metal−organic frameworks (MOFs) have demonstrated high selectivity toward CO_2 gas because of their high surface areas and chemically adjustable functionalities.[5] In comparison with the recently reported studies on the amine-functionalized MOFs,[6] the amide group is also able to provide attraction between the amide groups and the adsorbed CO_2 molecules by NC═O···CO_2 and NH···OCO interactions. However, amide-mediated MOFs used for effective CO_2 capture are far less common than the amine-mediated MOFs.[6a,f]

As part of our ongoing efforts in the design and synthesis of functional crystalline materials,[7] we wish to report herein on the synthesis, structure, and unique CO_2 adsorption behavior of a porous MOF, $\{[Zn_4(BDC)_4(BPDA)_4]\cdot 5DMF\cdot 3H_2O\}_n$ (**1**, BDC = 1,4-benzyl dicarboxylate, BPDA = *N*,*N*′-bis(4-pyridinyl)-1,4-benzenedicarboxamide), formed from 4^4-**sql** $[Zn_4(BDC)_4]$ layers and a long pillar of BPDA. The features of this material are as follows: (i) a porous MOF containing amide-functionalized open-ended channels, (ii) the amide groups in **1** provide a good cooperative effect for effectively capturing CO_2, which permits the perfect arrangement of CO_2 molecules, (iii) compound **1** displays high isosteric heat of CO_2 adsorption (Q_{st}), which significantly increases with increasing CO_2 uptake, (iv) DFT calculations revealed the optimal 1:1 ratio of the amide active sites to the adsorbed CO_2 molecules can exist at ambient condition because of the unique belt-like arrangement of the ulsheltered amide groups. To the best of our knowledge, this unique spatial arrangement for CO_2 adsorption has never been reported in the literature.

Received: December 15, 2012
Published: March 20, 2013

   dx.doi.org/10.1021/ic302758g | *Inorg. Chem.* 2013, 52, 3962−3968

RESULTS AND DISCUSSION

Synthesis. Compound **1** was synthesized by reacting $ZnCl_2$, 1,4-benzyl dicarboxylic acid (H_2BDC), and *N*,*N*′-bis(4-pyridinyl)-1,4-benzenedicarboxamide (BPDA) in a DMF/H_2O solution under hydrothermal conditions at 120 °C for 72 h through a single-step self-assembly process (Scheme 1).

Scheme 1. Synthesis of Compound 1 by a One-Step Self-Assembly Process

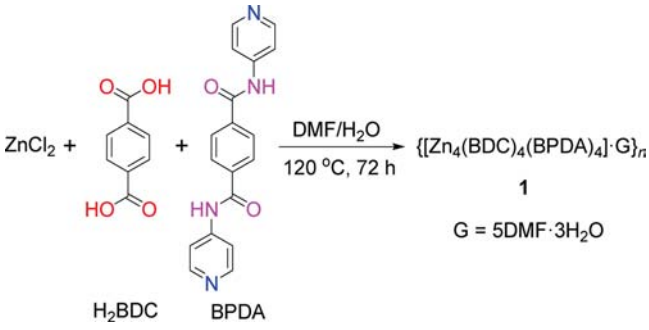

The appropriate choice of two mutually complemented organic scaffolds is a major factor in achieving the target structure. The BPDA ligand, an elongated ancillary linker, was deliberately synthesized so as to contain amide functional groups. Unlike ubiquitous bipyridine linkers, this amide-functionalized scaffold can drastically enhance the amount of CO_2 stored in MOF materials.[6a,f,g]

Description of the Crystal Structure. Single-crystal X-ray diffraction analysis revealed that compound **1** crystallizes in the monoclinic space group $P2_1/c$ (Table S1, Supporting Information).[8] The asymmetric unit consists of four Zn(II) atoms, four BDC^{2-} ligands, four BPDA linkers, five DMF, and three water guest molecules. The framework is constructed from a six-connected dinuclear $\{Zn_2N_4O_6\}$ node, which is octahedrally bound to four BDC ligands and two double-BPDA-deckered pillars (Figures 1a and 1b). This SBU resembles a two-blade paddlewheel. The Zn−N bond lengths are in the range of 2.131(7)−2.204(8) Å, and the Zn−O bond lengths are in the range of 1.967(6)−2.014(6) Å (Table S1, Supporting Information). Each BDC^{2-} ligand acts as a μ_3-bridge to link three Zn(II) atoms, in which one carboxylate group exhibits a μ_2-η_1:η_1-bridging coordination mode, while the other adopts a monodentate structure (Figure 1b). Due to the different coordination modes of the carboxylate group of the dizinc(II) node, the 4^4-**sql** layer of $[Zn_4(BDC)_4]$ has dimensions of 12.546 × 12.443 Å^2. The pillared length of the BDPA linker between the $[Zn_4(BDC)_4]$ layer is 20.18 Å. The overall array of the framework results in a $4^{12}\cdot6^3$-**pcu** topology, a high-symmetry uninodal six-connected net (Figure 1c).

Because each **pcu**-type net in **1** is quite large, the two identical nets are mutually interpenetrated (Figure 1c). The BPDA ligand exhibits strong net-to-net and host−guest hydrogen-bonding interactions.[7b,9] The amide groups of the BPDA ligand show moderate N−H···O hydrogen-bonding interactions (N···O = 2.89 Å) with the carboxylate oxygen atom of the BDC^{2-} ligand. The net-to-net interactions aid in stabilizing the mutually interpenetrating nets (Figure 2a). A perspective view of the porous framework reveals two different channel openings with effective dimensions of 2 × 3 and 3 × 9 Å^2, respectively. These cavities contain at least 20 DMF molecules and 12 H_2O molecules per unit cell. In spite of the 2-fold interpenetration, an analysis using the PLATON[10a] software tool indicates that the extra-framework volume per unit cell for **1** is approximately 29%. After removing all guest molecules, the amide groups of the framework are apparently unsheltered and regularly arranged inside the larger channels in **1** (Figure 2c).

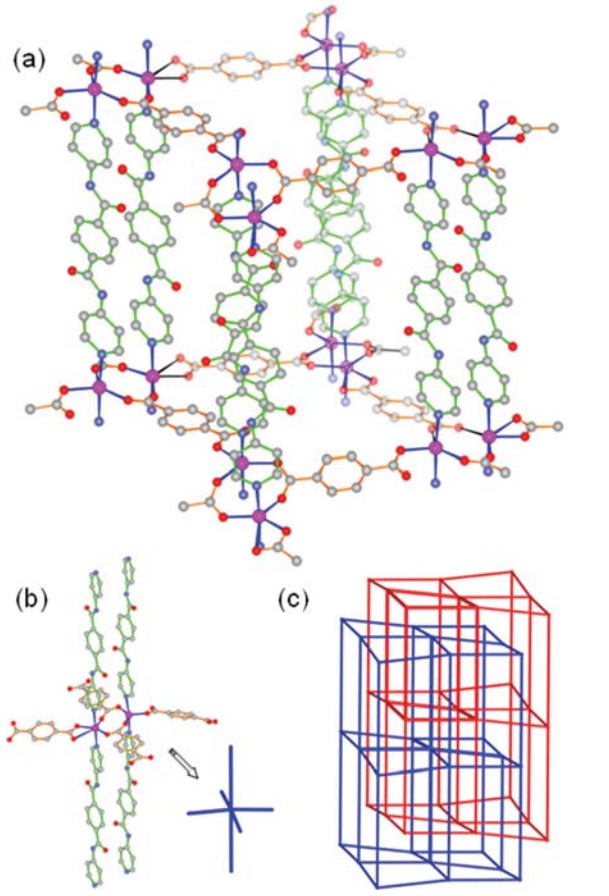

Figure 1. Structures of **1**: (a) Side view of an α-polonium-type cage; (b) simplified view of a six-connected node; (c) 2-fold interpenetrated $4^{12}\cdot6^3$ net.

Thermogravimetric Analysis (TGA) and Powder X-ray Diffraction (PXRD) Studies. Thermogravimetric analysis of **1** showed that guest molecules are eliminated from the network (calcd 16.1%; found 16.5%, which correspond to loss of 20 DMF molecules and 12 H_2O molecules per unit cell) when the temperature is increased from room temperature to about 270 °C (Figure S5, Supporting Information). PXRD patterns recorded using solid samples of **1** at room temperature are in good agreement with the simulated patterns calculated from single-crystal structure data.[10b] Even after drying at 150 °C for 1 day, compound **1** retained acceptable crystallinity, as evidenced by the measured PXRD patterns (Figure S4, Supporting Information).

Gas Adsorption and Selectivity. Prior to gas adsorption experiments, we prepared samples of **1**′ in which DMF had been removed. These samples were further degassed at 150 °C for 1 day under high vacuum. Evaluated compound **1** was used in studies of gas adsorption behavior. N_2 adsorption isotherms showed only a minor uptake at 77 K (Figure 3a). The low N_2 adsorption may be due to possible framework contraction and no appropriate intermolecular interactions at low temperature.[9a] The CO_2 adsorption for **1** at 195 K exhibited a

dx.doi.org/10.1021/ic302758g | Inorg. Chem. 2013, 52, 3962−3968

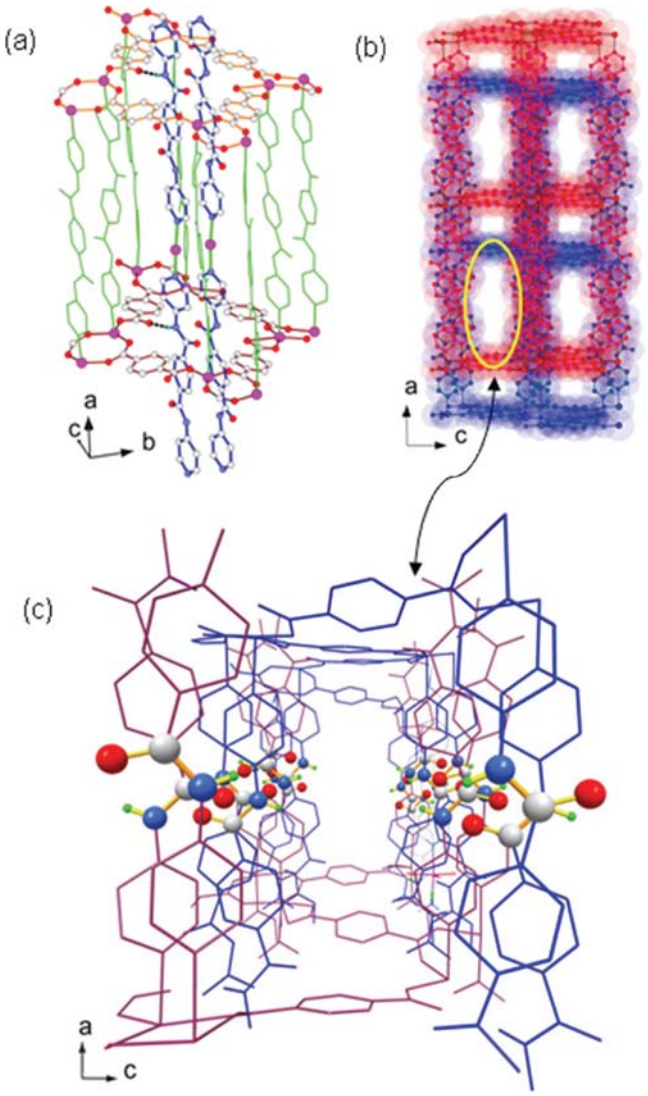

Figure 2. (a) Net-to-net N−H···O hydrogen-bonding interactions in **1**. (b) Superimposed space-filling representation of **1** showing two different sized channels. (c) Spotlight of the larger channel opening showing a nearly unique arrangement of the unsheltered amide groups in **1**.

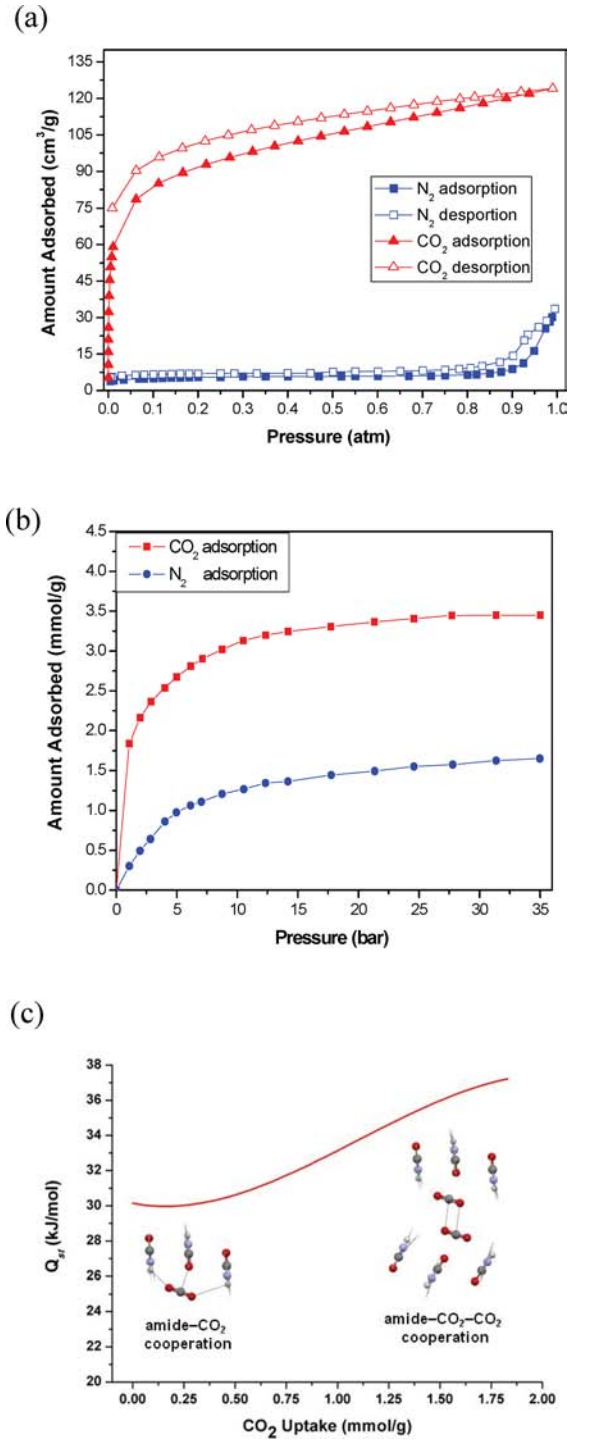

Figure 3. Adsorption properties of **1**: (a) adsorption isotherms of N_2 and CO_2 measured at 77 and 195 K, respectively; (b) adsorption isotherms of N_2 and CO_2 measured at 298 K and high pressure, respectively; (c) isosteric heat (Q_{st}) of CO_2 adsorption.

reversible type I isotherm (Figure 3a), which is characteristic of microporous materials. The estimated apparent Brunauer−Emmett−Teller (BET) surface area was ~331 m^2 g^{-1} (Langmuir surface ≈ 468 m^2 g^{-1}). Compound **1** takes up 3.45 mmol/g of CO_2 and 1.65 mmol/g of N_2 at 35 bar and takes up 1.84 mmol/g of CO_2 and 0.31 mmol/g of N_2 at 298 K and 1 bar (Figure 3b). As shown in Figure 3b, **1** displayed a distinct selective adsorption capacity for CO_2 over N_2 at 298 K and low pressure. Interestingly, the amount of captured CO_2 molecules at 1 bar is nearly equivalent to the number of exposed amide groups of the framework. This fact implies that the amide groups inside the framework are involved in efficient intermolecular interactions with the adsorbed CO_2 molecules (their ratio is near 1:1) at ambient pressure and temperature (Scheme S1, Supporting Information). This is a fairly novel example that is rarely seen in a host−guest adsoption system. The basic interactions between amide groups and adsorbed CO_2 molecules is of fundamental importance. To the best of our knowledge, this finding is reported for the first time. To better understand these observations, we calculated the isosteric heat of CO_2 adsorption (Q_{st}) of **1** by the virial method,[11a,b] which exhibits a strong binding affinity for CO_2 (30.2 kJ mol^{-1}) at zero coverage. It is uncommon that Q_{st} for **1** exhibits a significant increase with increasing CO_2 uptake from 30.2 to 37.2 kJ mol^{-1} (Figure 3c), depending on the adsorbed amount of CO_2 molecules. Theoretical analysis was therefore conducted to explore the details. The Q_{st} of **1** is close to NJU-Bai3 (36.5 kJ

dx.doi.org/10.1021/ic302758g | Inorg. Chem. 2013, 52, 3962−3968

mol^{-1})[6f] and higher than $[Cu_{24}(TPBTM^{6-})_8(H_2O)_{24}]$ (26.3 kJ mol^{-1}),[6a] $Cu_3(BTB^{6-})$ (24.1 kJ mol^{-1}), and $Cu_3(TATB^{6-})$ (24.4 kJ mol^{-1}).[6g]

Theoretical Calculations. To gain insight into the adsorption mode and origin of the 1:1 amide:CO_2 adsorption ratio at ambient condition, density functional theory (DFT) calculations were carried out.[5e,12] It can be seen from the molecular electrostatic potential of a fragment of **1** that the exposed amide groups in the large channels form belts of alternating polarity (Figures 2c and 4a), with the amide hydrogen atom (blue in Figure 4) protruding from the belt by roughly 1 Å relative to the amide oxygen atom (yellow in Figure 4). These belts would be predicted to be the most favorable area in the channel to attract the electropositive (C) and electronegative (O) sites of CO_2. Calculations of binding energies were carried out for CO_2 and a fragment of **1** (termed model a, Figure 4b) consisting of three (4-pyridyl)benzamide aligned in coordinates found in the crystal structure of **1**. Model a was used to calculate the binding energy because its electrostatic potential was similar to that in the larger fragment of **1** (Figure 4).

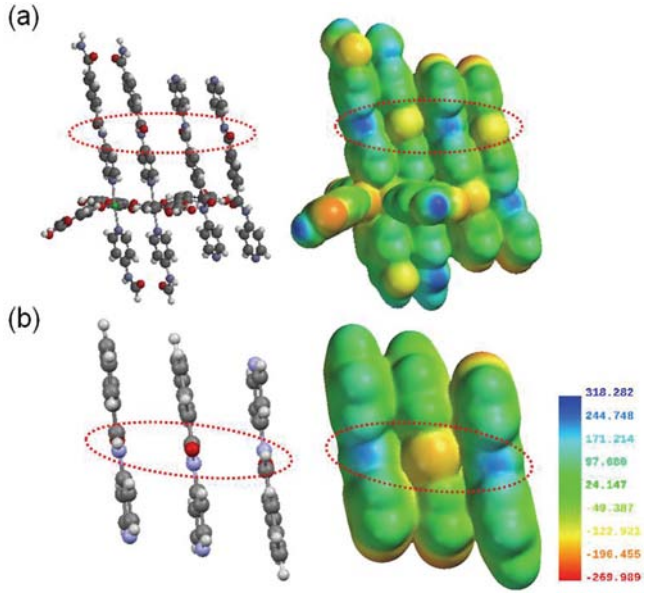

Figure 4. (a) Atomic structure of a fragment of **1** and its electrostatic potential map. (b) Atomic structure of model a and its electrostatic potential map. (In ball and stick style; C = gray; H = white; O = red; N = blue; Zn = green). Exposed amide groups are marked by red dashed circles. Colors of the electrostatic potential map, ranging from red to blue, correspond to electrostatic potential ranging from −269.989 to 318.282 kJ mol^{-1}. Red, green, and blue represent negative, zero, and positive values, respectively.

The largest binding energy calculated at the M06-2X/6-31++G(2d,2p)//M06-2X/6-31G(d,p) level was −28.4 kJ mol^{-1} for the CO_2·model a, where model a was frozen at the corresponding X-ray structure of **1** and CO_2 was fully optimized starting from different initial positions. This binding energy is of similar magnitude to the Q_{st} at zero coverge (30.2 kJ mol^{-1}). The lowest energy structure of CO_2·model a showed intermolecular C···O and O···H distances of 2.55 and 2.41 Å with the middle and left (4-pyridyl)benzamide, respectively (Figures 5a and 5b). The CO_2 molecule was slightly nonlinear (175.8°) when bound to model a. As the above O···H distance (2.41 Å) was much longer than that of a normal hydrogen bond, the major source of attraction should be from a Lewis acid−Lewis base interaction between the CO_2 carbon atom and the amide oxygen atom of the middle (4-pyridyl)benzamide. Frozen in the optimized geometry of the CO_2·model a, interaction energies of CO_2 with individual (4-pyridyl)-benzamide were found to be −7.3, −11.1, and −2.8 kJ mol^{-1} with the left, middle, and right (4-pyridyl)benzamide shown in Figure 5, respectively. As expected, CO_2 interacted most strongly with the middle (4-pyridyl)benzamide. On the other hand, the right (4-pyridyl)benzamide unit contributed to the binding as well, rather than not participating in the binding. The binding energy of CO_2·model a was 7.2 kJ mol^{-1} more negative than the sum of the three individual interaction energies (−21.2 kJ mol^{-1}). Therefore, the amide belt offered an environment for cooperative binding. When both the left and the middle (4-pyridyl)benzamide were held in the X-ray coordinates and interacted with a CO_2 molecule, the overall CO_2 binding energy (−24.0 kJ mol^{-1}) was 5.6 kJ mol^{-1} more negative than the sum of the individual CO_2 binding energies

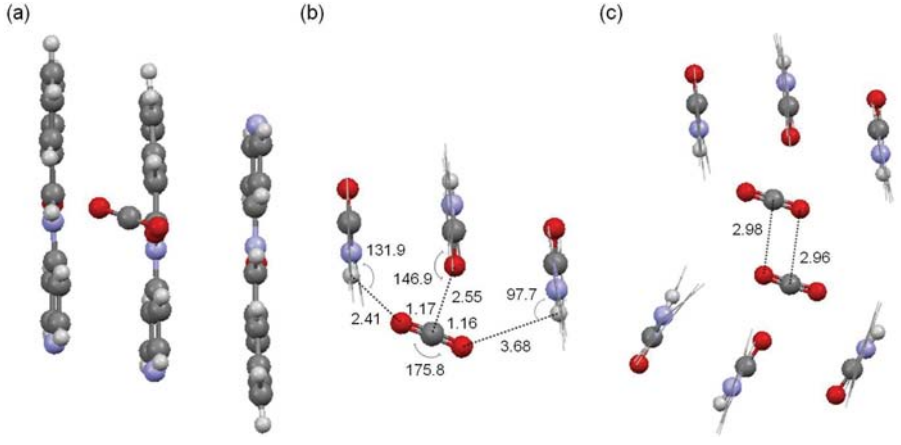

Figure 5. (a) Side view of the M06-2X/6-31G**-optimized structure of CO_2·model a shown with a ball and stick representation, and (b) geometry parameters labeled on the top view of the same complex shown in the wireframe representation, except that the amide groups and CO_2 are in ball and stick style. (c) Top view of the optimized structure of the $2CO_2$·model b complex calculated at the M06-2X/6-31G** level. Amide groups and CO_2 are in ball and stick representation (distances are in Angstroms and angles in degrees).

dx.doi.org/10.1021/ic302758g | Inorg. Chem. 2013, 52, 3962−3968

(−7.3 and −11.1 kJ mol^{-1}). The calculated cooperativity of binding is reasonable. When a Lewis base donates an electron to the electron-deficient carbon atom in CO_2 the CO_2 oxygen atoms become more electron rich, resulting in formation of stronger hydrogen bonds. A recent high-level theoretical study on small model systems of CO_2 also showed similar cooperative binding as described above.[13]

As shown in Figure 5c, six (4-pyridyl)benzamide molecules (termed model b) were held in the X-ray structure of the major channel to simulate the vertical walls of the channel. It was found that two CO_2 molecules can fit snugly between the walls, affording an interaction energy of $2CO_2$·model b of −61.8 kJ mol^{-1}, a value more than twice that of CO_2·model a. A single-point calculation revealed that the slipped-parallel disposition found in $2CO_2$·model b provided an attraction of −2.9 kJ mol^{-1} between the two CO_2 molecules. It should be noted that high-level theoretical calculations[14] and experimental studies[15] revealed that the gas-phase global minimum structure of a CO_2 dimer is slipped parallel. The same geometric feature has also been observed in CO_2 crystals.[16] In the crystal structure of **1**, the N−H and C═O groups of the exposed amide groups are pointing to opposite directions. While the amide hydrogen atom interacts with a CO_2 oxygen atom in one channel, the oxygen atom of the same amide group interacts with a CO_2 carbon atom in the next channel. Because the exposed amide group and CO_2 each provide two binding sites for amide:CO_2 binding, a 1:1 adsorption ratio at ambient condition is observed. Overall, the calculations showed that **1** provides belts of interaction sites for cooperative binding not only for CO_2·amide binding but also for CO_2·CO_2 binding. These findings help to explain the observed increase of Q_{st} from low to 1:1 CO_2 uptake.

CONCLUSION

An intriguing spatial arrangement of amide groups inside the open-ended channels of **1** is reported. A 1:1 ratio of amide sorption sites to CO_2 molecules at low pressure (1 bar) and ambient temperature is observed for this material. The isosteric heat of CO_2 adsorption (Q_{st}) for **1** exhibits a significant increase with increasing CO_2 uptake. Theoretical analysis suggested that the channels of compound **1** provide belts of interaction sites for cooperative binding not only for CO_2·amide binding but also for CO_2·CO_2 binding. This type of spatial arrangement of CO_2 adsorption sites has not been reported before.

EXPERIMENTAL SECTION

Materials and Instruments. *N*,*N*′-Bis(4-pyridinyl)-1,4-benzenedicarboxamide (BPDA) was synthesized as reported previously.[6] Other chemicals were purchased commercially and used as received without further purification. Thermogravimetric analyses were performed under nitrogen with a Perkin-Elmer TGA-7 TG analyzer. Powder X-ray diffraction measurements were recorded at room temperature on a Siemens D-5000 diffractometer at 40 kV, 30 mA for Cu Kα (λ = 1.5406 Å) with a step size of 0.02° in θ and a scan speed of 1 s per step size. Elemental analyses (C, H, N) were carried out on a Perkin-Elmer 2400 CHN elemental analyzer. Brunauer−Emmett−Teller analyses were investigated with a Micrometrics ASAP 2020 system using nitrogen as the adsorbate at 77 K and carbon dioxide as the adsorbate at 195 K, 273 K, and 298 K. The high-pressure gas adsorption isotherms were investigated with a thermo D110 balance in the high-pressure installation using nitrogen and carbon dioxide as adsorbates at 298 K. All gases used were of 99.9995% purity.

Synthesis of {[Zn_4(BDC)$_4$(BPDA)$_4$]·5DMF·3H_2O}$_n$ (1). A mixture of $ZnCl_2$ (20.5 mg, 0.15 mmol), H_2BDC (24.9 mg, 0.15 mmol), BPDA (47.8 mg, 0.15 mmol), DMF (7 mL), and H_2O (0.5 mL) was sealed in a Teflon-lined stainless steel Parr acid digestion bomb and heated at 120 °C for 72 h and then slowly cooled to 30 °C. Colorless block crystals of compound **1** were formed in 51% yield (50.5 mg, based on $ZnCl_2$). Solid product was isolated on a filter, and crystals were then washed with water and dried in air. Anal. Calcd for $C_{119}H_{113}N_{21}O_{32}Zn_4$ = [Zn_4(BDC)$_4$(BPDA)$_4$]·5DMF·3H_2O: C, 54.74; H, 4.36; N, 11.27. Found: C, 54.86; H, 4.38; N, 10.88. IR (KBr): ν = 3363 (m), 3317 (m), 3084 (m), 1674 (s), 1595 (vs), 1511 (vs), 1430 (s), 1389 (s), 1364 (s), 1332 (s), 1299 (s), 1268 (m), 1213 (s), 1146 (w), 1115 (m), 1066 (w), 1028 (m), 1017 (w), 888 (w), 866 (w), 833 (m), 750 (m), 714 (m), 667 (w), 614 (m), 614 (m), 538 (m) cm^{-1}.

Crystallographic Determination. A suitable single crystal of **1** was mounted on the tip of a glass fiber with dimensions of 0.28 × 0.25 × 0.25 mm^3 and placed onto the goniometer head for indexing and intensity data collection using a Nonius Kappa CCD diffractometer equipped with graphite-monochromatized Mo Kα radiation (λ = 0.71073 Å). Collection of intensity data was conducted at 150 K. Empirical absorptions were applied using the multiscan method. The structure was solved by direct methods and refined against F^2 by the full-matrix least-squares technique using the SHELX-97 software packages.[17] The exact positions of the atoms in the BPDA ligands could not be successfully located, which is indicative of the high disorder in the relative orientation of the BPDA ligands. This fact is also reflected in the relatively high final residual values (R_1 = 11.7%, wR_2 = 31.8%). The phenyl rings and pyridyl rings of the BPDA ligand are disordered with 50% site occupancy (Figure S3, Supporting Information).

Computational Details. The BSSE-corrected binding energy (E_{corr}) of CO_2·formamide complex at the M06-2X, ωB97X-D, B97-D, B3LYP, and MP2 levels using various basis sets had been calculated and compared to that calculated at the level of CCSD(T)/aug-cc-pVTZ//MP2/aug-cc-pVTZ (18.5 kJ mol^{-1}). The theory level of M06-2X/6-31++G(2d,2p)//M06-2X/6-31G(d,p) was chosen to study larger systems because its CO_2·formamide binding energy, 20.1 kJ mol^{-1}, was quite close to the CCSD(T) result. For dimerization energy of slipped-parallel CO_2, the chosen level affords 5.1 kJ mol^{-1}, also comparing well to that of the CCSD(T)/CBS result, 6.2 kJ mol^{-1}.[14a] All model structures related to **1** were constructed from its crystallographic data. Model a (Figure 5b) consists of three (4-pyridyl)benzamide molecules, and model b (Figure 5c) consists of six (4-pyridyl)benzamide molecules, representing the vertical walls of the larger channel in **1**. Electrostatic potential maps were calculated at the M06-2X/6-31G* level with Spartan '08[18] (isovalue, 0.002; resolution, high). Except for calculation of the electrostatic potential, all other calculations were performed using the Gaussian 09 program.[19] Optimized structures of CO_2·model a and $2CO_2$·model b complexes were obtained at the M06-2X/6-31G** level (Int(grid = ultrafine)) with frozen models a/b to mimic the crystal state of **1**. The binding energies of CO_2·model a and $2CO_2$·model b complexes were then calculated at the M06-2X/6-31++G(2d,2p) level using the ultrafine grid option. The basis set superposition errors (BSSE) in calculated binding energy were eliminated with the counterpoise method (CP) of Boys and Bernardi.[20] When calculating BSSE, model a/b, the first carbon dioxide, and the second carbon dioxide were regarded as the first, second, and third fragment in the complex, respectively. For CO_2·model a complex, we tested three initial structures; CO_2 was placed close to the left, middle, and right (4-pyridyl)benzamide. After geometry optimization, the binding energies were found to be −28.4, −27.8, and −27.8 kJ mol^{-1}, respectively. All three optimized structures (two converged to nearly the same geometry) were of similar feature in that a short C···O contact was found, accompanied by an elongated O···H hydrogen bond. Only the first result was presented in the Results and Discussion section.

dx.doi.org/10.1021/ic302758g | Inorg. Chem. 2013, 52, 3962−3968

■ ASSOCIATED CONTENT

Supporting Information

Crystallographic data (CIF), structural pictures, PXRD patterns, TGA data, CO_2 adsorption isothermals of **1**, isosteric heat (Q_{st}). This material is available free of charge via the Internet at http://pubs.acs.org.

■ AUTHOR INFORMATION

Corresponding Author

*E-mail: ichao@gate.sinica.edu.tw (I.C.); kllu@gate.sinica.edu.tw (K.-L.L.).

Notes

The authors declare no competing financial interest.

■ ACKNOWLEDGMENTS

We are grateful to Academia Sinica and the National Science Council of Taiwan for financial support. We also thank the National Center for High-performance Computing (NCHC) and Academia Sinica Computing Center (ASCC) for providing computational resources.

■ REFERENCES

(1) (a) Kintisch, E. *Science* **2007**, *317*, 184−186. (b) Cox, P.; Jones, C. *Science* **2008**, *321*, 1642−1644. (c) D'Alessandro, D. M.; Smit, B.; Long, J. R. *Angew. Chem., Int. Ed.* **2010**, *49*, 6058−6082.

(2) (a) Millward, A. R.; Yaghi, O. M. *J. Am. Chem. Soc.* **2005**, *127*, 17998−17999. (b) Maji, T. K.; Mostafa, G.; Matsuda, R.; Kitagawa, S. *J. Am. Chem. Soc.* **2005**, *127*, 17152−17153. (c) Lastoskie, C. *Science* **2010**, *330*, 595−596. (d) Li, J. R.; Kuppler, R. J.; Zhou, H.-C. *Chem. Soc. Rev.* **2009**, *38*, 1477−1504. (e) Farha, O. K.; Yazaydın, A. Ö.; Eryazici, I.; Malliakas, C. D.; Hauser, B. G.; Kanatzidis1, M. G.; Nguyen, S. T.; Snurr, R. Q.; Hupp, J. T. *Nature Chem.* **2010**, *2*, 944−948. (f) Bae, Y.-S.; Snurr, R. Q. *Angew. Chem., Int. Ed.* **2011**, *50*, 11586−11596.

(3) (a) Rochelle, G. T. *Science* **2009**, *325*, 1652−1654. (b) Radosz, M.; Hu, X.; Krutkramelis, K.; Shen, Y. *Ind. Eng. Chem. Res.* **2008**, *47*, 3783−3794.

(4) (a) Yan, X.; Zhang, L.; Zhang, Y.; Yang, G.; Yan, Z. *Ind. Eng. Chem. Res.* **2011**, *50*, 3220−3226. (b) Tang, Y.; Landskron, K. *J. Phys. Chem. C* **2010**, *114*, 2494−2498. (c) Knowles, G. P.; Graham, J. V.; Delaney, S. W.; Chaffee, A. L. *Fuel Process. Technol.* **2005**, *86*, 1435−1448.

(5) (a) Vaidhyanathan, R.; Iremonger, S. S.; Dawson, K. W.; Shimizu, G. K. H. *Chem. Commun.* **2009**, 5230−5232. (b) Demessence, A.; D'Alessandro, D. M.; Foo, M. L.; Long, J. R. *J. Am. Chem. Soc.* **2009**, *131*, 8784−8786. (c) Zhao, Y.; Wu, H.; Emge, T. J.; Gong, Q.; Nijem, N.; Chabal, Y. J.; Kong, L.; Langreth, D. C.; Liu, H.; Zeng, H.; Li, J. *Chem.—Eur. J.* **2011**, *17*, 5101−5109. (d) Zou, Y.; Hong, S.; Park, M.; Chun, H.; Lah, M. S. *Chem. Commun.* **2007**, 5182−5184. (e) Vaidhyanathan, R.; Iremonger, S. S.; Shimizu, G. K. H.; Boyd, P. G.; Alavi, S.; Woo, T. K. *Science* **2010**, *330*, 650−653.

(6) (a) Zheng, B.; Bai, J.; Duan, J.; Wojtas, L.; Zaworotko, M. J. *J. Am. Chem. Soc.* **2011**, *133*, 748−751. (b) Tzeng, B.-C.; Chiu, T.-H.; Chen, B.-S.; Lee, G.-H. *Chem.—Eur. J.* **2008**, *14*, 5237−5245. (c) Hasegawa, S.; Horike, S.; Matsuda, R.; Furukawa, S.; Mochizuki, K.; Kinoshita, Y.; Kitagawa, S. *J. Am. Chem. Soc.* **2007**, *129*, 2607−2614. (d) Adarsh, N. N.; Kumar, D. K.; Dastidar, P. *CrystEngComm* **2009**, *11*, 796−802. (e) Song, X.; Zou, Y.; Liu, X.; Oh, M.; Lah, M. S. *New J. Chem.* **2010**, *34*, 2396−2399. (f) Duan, J.; Yang, Z.; Bai, J.; Zheng, B.; Li, Y.; Li, S. *Chem. Commun.* **2012**, *48*, 3058−3060. (g) Zheng, B.; Yang, Z.; Bai, J.; Li, Y.; Li, S. *Chem. Commun.* **2012**, *48*, 7025−7027.

(7) (a) Luo, T. T.; Wu, H. C.; Jao, Y. C.; Huang, S. M.; Tseng, T. W.; Wen, Y. S.; Lee, G. H.; Peng, S. M.; Lu, K. L. *Angew. Chem.* **2009**, *121*, 9625−9628; *Angew. Chem., Int. Ed.* **2009**, *48*, 9461−9464. (b) Luo, T. T.; Tsai, H. L.; Yang, S. L.; Liu, Y. H.; Yadav, R. D.; Su, C. C.; Ueng, C. H.; Lin, L. G.; Lu, K. L. *Angew. Chem.* **2005**, *117*, 6217−6221; *Angew. Chem., Int. Ed.* **2005**, *44*, 6063−6067. (c) Thanasekaran, P.; Luo, T. T.; Lee, C. H.; Lu, K. L. *J. Mater. Chem.* **2011**, *21*, 13140−13149.

(8) Crystal structure data for **1**: $C_{119}H_{113}N_{21}O_{32}Zn_4$ $\{[Zn_4(BDC)_4(BPDA)_4]\cdot 5DMF\cdot 3H_2O\}_n$, M_r = 2610.78, monoclinic, $P2_1/c$, a = 20.1818(3) Å, b = 30.2868(5) Å, c = 19.7451(3) Å, β = 90.6880(6)°, V = 12068.2(3) Å^3, Z = 4, ρ_{calcd} = 1.437 g cm^{-3}, μ = 0.873 mm^{-1}, λ (Mo Kα) = 0.71073 Å, $F(000)$ = 5392, T = 150(1) K. Final R indices: R_1 = 0.1169, wR_2 = 0.3184 for 18 113 reflections [$I > 2\sigma(I)$]; R_1 = 0.1300, wR_2 = 0.3261 for 21 222 independent reflections (all data) and 1496 parameters, GOF = 1.384. CCDC 881631 (**1**) contains the supplementary crystallographic data for this paper. These data can be obtained free of charge from the Cambridge Crystallographic Data Centre via www.ccdc.cam.ac.uk/data_request/cif.

(9) (a) Lin, J.-B.; Zhang, J.-P.; Chen, X.-M. *J. Am. Chem. Soc.* **2010**, *132*, 6654−6656. (b) Comotti, A.; Bracco, S.; Sozzani, P.; Horike, S.; Matsuda, R.; Chen, J.; Takata, M.; Kubota, Y.; Kitagawa, S. *J. Am. Chem. Soc.* **2008**, *130*, 13664−13672.

(10) (a) Spek, A. L. *J. Appl. Crystallogr.* **2003**, *36*, 7−13. (b) Kubota, Y.; Takata, M.; Matsuda, R.; Kitaura, R.; Kitagawa, S.; Kobayashi, T. C. *Angew. Chem., Int. Ed.* **2006**, *45*, 4932−4936.

(11) (a) Rowsell, J. L. C.; Yaghi, O. M. *J. Am. Chem. Soc.* **2006**, *128*, 1304−1315. (b) Sumida, K.; Rogow, D. L.; Mason, J. A.; McDonald, T. M.; Bloch, E. D.; Herm, Z. R.; Bae, T.-H.; Long, J. R. *Chem. Rev.* **2012**, *112*, 724−781.

(12) (a) Ramsahye, N. A.; Maurin, G.; Bourrelly, S.; Llewellyn, P. L.; Loiseau, T.; Férey, G. *Phys. Chem. Chem. Phys.* **2007**, *9*, 1059−1063. (b) Ramsahye, N. A.; Maurin, G.; Bourrelly, S.; Llewellyn, P. L.; Serre, C.; Loiseau, T.; Devic, T.; Férey, G. *J. Phys. Chem. C* **2008**, *112*, 514−520.

(13) Lange, K. M.; Lane, J. R. *J. Chem. Phys.* **2011**, *135*, 064304-1−064304-8.

(14) (a) McMahon, J. D.; Lane, J. R. *J. Chem. Phys.* **2011**, *135*, 15430911−154309-9. (b) Bukowski, R.; Sadlej, J.; Jeziorski, B.; Jankowski, P.; Szalewicz, K.; Kucharski, S. A.; Williams, H. L.; Rice, B. M. *J. Chem. Phys.* **1999**, *110*, 3785−3803. (c) Tsuzuki, S.; Klopper, W.; Lüthi, H. P. *J. Chem. Phys.* **1999**, *111*, 3846−3854.

(15) (a) Walsh, M. A.; England, T. H.; Dyke, T. R.; Howard, B. J. *Chem. Phys. Lett.* **1987**, *142*, 265−270. (b) Jucks, K. W.; Huang, Z. S.; Dayton, D.; Miller, R. E.; Lafferty, W. J. *J. Chem. Phys.* **1987**, *86*, 4341−4346. (c) Jucks, K. W.; Huang, Z. S.; Miller, R. E.; Fraser, G. T.; Pine, A. S.; Lafferty, W. J. *J. Chem. Phys.* **1988**, *88*, 2185−2195.

(16) Yoo, C. S.; Kohlmann, H.; Cynn, H.; Nicol, M. F.; Iota, V.; LeBihan, T. *Phys. Rev. B* **2002**, *65*, 104103-1−104103-6.

(17) Sheldrick, G. M. *Acta Crystallogr., Sect. A* **2008**, *64*, 112−122.

(18) Spartan'08 Wavefunction, Inc. Irvine, CA Except for molecular mechanics and semi-empirical models, calculation methods used in Spartan have been documented, see: Shao, Y.; Molnar, L. F.; Jung, Y.; Kussmann, J.; Ochsenfeld, C.; Brown, S. T.; Gilbert, A. T. B.; Slipchenko, L. V.; Levchenko, S. V.; O'Neill, D. P.; DiStasio, R. A., Jr.; Lochan, R. C.; Wang, T.; Beran, G. J. O.; Besley, N. A.; Herbert, J. M.; Lin, C. Y.; Van Voorhis, T.; Chien, S. H.; Sodt, A.; Steele, R. P.; Rassolov, V. A.; Maslen, P. E.; Korambath, P. P.; Adamson, R. D.; Austin, B.; Baker, J.; Byrd, E. F. C.; Dachsel, H.; Doerksen, R. J.; Dreuw, A.; Dunietz, B. D.; Dutoi, A. D.; Furlani, T. R.; Gwaltney, S. R.; Heyden, A.; Hirata, S.; Hsu, C.-P.; Kedziora, G.; Khalliulin, R. Z.; Klunzinger, P.; Lee, A. M.; Lee, M. S.; Liang, W. Z.; Lotan, I.; Nair, N.; Peters, B.; Proynov, E. I.; Pieniazek, P. A.; Rhee, Y. M.; Ritchie, J.; Rosta, E.; Sherrill, C. D.; Simmonett, A. C.; Subotnik, J. E.; Woodcock, H. L., III; Zhang, W.; Bell, A. T.; Chakraborty, A. K.; Chipman, D. M.; Keil, F. J.; Warshel, A.; Hehre, W. J.; Schaefer, H. F.; Kong, J.; Krylov, A. I.; Gill, P. M. W.; Head-Gordon, M. *Phys. Chem. Chem. Phys.* **2006**, *8*, 3172−3191.

(19) Frisch, M. J.; Trucks, G. W.; Schlegel, H. B.; Scuseria, G. E.; Robb, M. A.; Cheeseman, J. R.; Scalmani, G.; Barone, V.; Mennucci, B.; Petersson, G. A.; Nakatsuji, H.; Caricato, M.; Li, X.; Hratchian, H. P.; Izmaylov, A. F.; Bloino, J.; Zheng, G.; Sonnenberg, J. L.; Hada, M.; Ehara, M.; Toyota, K.; Fukuda, R.; Hasegawa, J.; Ishida, M.; Nakajima, T.; Honda, Y.; Kitao, O.; Nakai, H.; Vreven, T.; Montgomery, Jr., J. A.;

Peralta, J. E.; Ogliaro, F.; Bearpark, M.; Heyd, J. J.; Brothers, E.; Kudin, K. N.; Staroverov, V. N.; Kobayashi, R.; Normand, J.; Raghavachari, K.; Rendell, A.; Burant, J. C.; Iyengar, S. S.; Tomasi, J.; Cossi, M.; Rega, N.; Millam, J. M.; Klene, M.; Knox, J. E.; Cross, J. B.; Bakken, V.; Adamo, C.; Jaramillo, J.; Gomperts, R.; Stratmann, R. E.; Yazyev, O.; Austin, A. J.; Cammi, R.; Pomelli, C.; Ochterski, J. W.; Martin, R. L.; Morokuma, K.; Zakrzewski, V. G.; Voth, G. A.; Salvador, P.; Dannenberg, J. J.; Dapprich, S.; Daniels, A. D.; Farkas, O.; Foresman, J. B.; Ortiz, J. V.; Cioslowski, J.; Fox, D. J. *Gaussian 09*, Revision A.02; Gaussian, Inc.: Wallingford, CT, 2009.

(20) Boys, S. F.; Bernardi, F. *Mol. Phys.* **1970**, *19*, 553−556.